Asociación Argentina
de Mecánica Computacional

Mecánica Computacional Vol XXXIV, págs. 3065-3073 (artículo completo)
Sebastián Giusti, Martín Pucheta y Mario Storti (Eds.)
Córdoba, 8-11 Noviembre 2016

INDUCED SEISMICITY IN UNCONVENTIONAL RESERVOIR USING A VISCOELASTIC MODEL FOR WAVE PROPAGATION

Lucas A. Macias[a], Juan E. Santos[b] and Gabriela B. Savioli[a]

[a]*Universidad de Buenos Aires, Facultad de Ingeniería, Instituto del Gas y del Petróleo, Laboratorio de Ingeniería de Reservorios, Buenos Aires, Argentina*

[b]*Universidad de Buenos Aires, Facultad de Ingeniería, Instituto del Gas y del Petróleo, Buenos Aires, Argentina and Department of Mathematics, Purdue University and Universidad Nacional de La Plata*

Keywords: Unconventional reservoirs, micro-seismicity, viscoelastic model.

Abstract. This work presents a first approach to study the fracture orientation during water injection in an unconventional gas reservoir. The fracture propagation process is based on a breakdown pressure criterion: once pore pressure becomes greater than the breakdown pressure on a certain cell, that cell is fractured and it can become a micro-seismic event. For a given spatial distribution of weak stress zones (related to the breakdown pore pressure criterion), the flow simulations allow to obtain different orientations of micro-seismic event distribution caused by water injection. In this work, the reservoir is consider to have a fractal distribution for porosity and permeability, while the petrophysical properties for the seismic modeling are computed applying the Krief equation. Using the spatio-temporal distribution of the micro-seismic events information, the viscoelastic model for wave propagation generates the corresponding synthetic seismograms for each orientations. Each evaluated scenario yields different responses, showing the potential of the technique to detect the fracture orientation during water injection.

1 INTRODUCTION

The process of injecting fluids at high pressure into a reservoir with the intention of producing fractures is known as hydraulic fracturing, or fracking. This process will also attempt to connect already existing natural fractures, creating pathways through which the hydrocarbons will flow to the wellbore (Riahi and Damjanac, 2013). Unconventional reservoirs, i.e. tight gas, tight oil, shale gas or shale oil, require this procedure because of their low permeability (Nagel et al., 2013).

Fluid injection during the fracking process increases the pore pressure until it reaches the breakdown value at which the in-situ effective pressure generates a fracture, triggering a micro-earthquake.

Tracking such events can help identify the fracture evolution within the reservoir together with its geometry. Longer-term micro-seismic monitoring has also been used to estimate reservoir permeability (Shapiro et al., 2005) (Shapiro et al., 1997). Such analysis can be done by adjusting the triggers envelope curve and obtaining the associated hydraulic diffusivity parameter (Rothert and Shapiro, 2003).

In this work the three-phase fluid flow Black-Oil model (Aziz and Settari, 1985) is used to simulate water injection into a gas reservoir in order to obtain an oriented micro-seismic event cloud. We also implement a viscoelastic wave propagation model to analyze the effect of the fracture orientation over the synthetic seismograms.

2 NUMERICAL MODEL OF WATER INJECTION

In order to simulate water injection, we apply the Black-Oil formulation to two-phase, two component fluid flow (Aziz and Settari, 1985). Our approach allows the gas component to dissolve in the water phase but the water cannot vaporize into the gas phase.

The model equations are obtained combining the mass conservation equation for each component with the empirical Darcy's law for each phase (Aziz and Settari, 1985). The thermodynamic behavior is simplified applying the PVT parameters: the gas solubility in water and the gas and water formation volume factors. Two differential equations are obtained: the pressure and saturation equations.

The numerical solution of the Black-Oil model was obtained employing the public domain software BOAST (Fanchi, 1997), which solves the differential equations using IMPES (IMplicit Pressure Explicit Saturation), a finite difference technique (Aziz and Settari, 1985). The system is discretized using a block centered grid and is linearized evaluating the pressure and saturation dependent coefficients at the previous time-step. The pressure equation is solved implicitly, applying a Block Successive Over Relaxation method (BSOR) to compute the linear system solution. The saturation equation is solved explicitly, therefore stability restrictions are considered to select the time step (Savioli and Bidner, 2005).

3 WATER INJECTION EXAMPLES

3.1 Reservoir Model

We consider a 2D section of an unconventional gas reservoir of 600 m in the horizontal direction and 200 m in the vertical direction located at a depth of 2210 m. The reservoir is considered isothermal and the initial pressure p_H is computed using equilibrium conditions. Gas properties are obtained from the Peng-Robinson equations as a function of temperature and pore pressure $p = S_w p_w + S_g p_g$ (Peng and Robinson, 1976).

We assume a fractal distribution for permeability (k) and porosity (ϕ), based on the Von-Kármán correlation function (Carcione and Gei, 2009), with average values of 0.5mD and 15% respectively and an initial gas saturation of 90%.

3.2 Fracture generation procedure

To simulate fracture propagation, we use the "breakdown pressure" criterion.

In this work, we employ several distributions for the breakdown pressure in order to generate different orientations for the fractures cloud, i.e., the zones of weaknesses are intentionally oriented in diverse directions to account for different scenarios.

The positions of the micro-seismic sources were determined using a fractal distribution for threshold pressures that indicate when the intensity of the breakdown is enough to generate a micro-earthquake.

3.3 Experiments

We simulate water injection at high pressure using a flow rate of 2000 STB/d during 5 hours. Three different scenarios were analyzed by changing the orientation of the zones of weakness. Figures 1, 2 and 3 show the micro-seismic sources distribution at $0°$, $45°$ and $90°$, respectively.

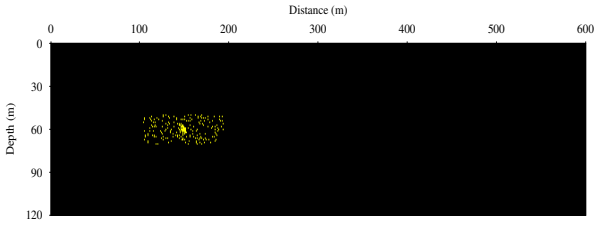

Figure 1: Micro-seismic events distribution at $0°$

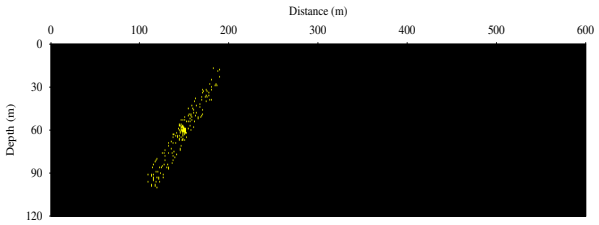

Figure 2: Micro-seismic events distribution at $45°$

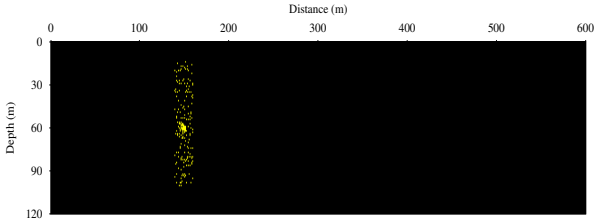

Figure 3: Micro-seismic events distribution at $90°$

4 SEISMIC MODEL

4.1 Mesoscopic attenuation effects

An important mechanism of P-wave attenuation and dispersion at seismic frequencies is known as mesoscopic loss, due to heterogeneities larger than the pore size but much smaller than the predominant wavelengths (mesoscopic-scale heterogeneities). Due to the extremely fine meshes needed to properly represent these type of media, numerical simulation at the macroscale is very expensive or even not feasible. Our approach to solve this problem consists in applying an upscaling procedure to include the mesoscale effects in the macroscale (Santos et al., 2011). Within the formation, in zones where gas is present, we determine complex and frequency dependent P-wave modulus $E(\omega) = \lambda(\omega) + 2\mu(\omega)$ at the mesoscale using White's theory for patchy saturation (White et al., 1975), where $\lambda(\omega)$ and $\mu(\omega)$ are the Lamé coefficients and ω is the angular frequency. Shear wave attenuation is taken into account using another relaxation mechanism, related to the P-wave White mechanism, to make the shear modulus $\mu(\omega)$ complex and frequency dependent. Outside the formation and in zones where only water is present, the complex bulk and shear moduli as function of frequency are determined using a Zener model. These complex moduli define an equivalent viscoelastic model at the macroscale that takes into account dispersion and attenuation effects occurring at the mesoscale.

4.2 Constitutive Relations

Let $u = u(\omega) = (u_x(\omega), u_z(\omega))$ be the time-Fourier transform of the displacement vector. Therefore, the stress-strain relations in the space-frequency domain are:

$$\sigma_{jk}(u) = \lambda(\omega)\nabla \cdot u\, \delta_{jk} + 2\mu(\omega)\varepsilon_{jk}(u), \tag{1}$$

where $\sigma_{jk}(u)$ is the stress tensor, $\varepsilon_{jk}(u)$ is the strain tensor, δ_{jk} is the Kronecker delta, and $\lambda(\omega), \mu(\omega)$ are the complex Lamé coefficients determined using White's theory.

For isotropic viscoelastic solids, the frequency dependent phase velocities $v_t(\omega)$ and quality factors $Q_t(\omega)$ $(t = p, s)$ are defined by the relations

$$v_t(\omega) = \left[\mathrm{Re}\left(\frac{1}{vc_t(\omega)}\right)\right]^{-1}, \; Q_t(\omega) = \frac{\mathrm{Re}(vc_t(\omega)^2)}{\mathrm{Im}(vc_t(\omega)^2)}, \tag{2}$$

where $vc_p(\omega), vc_s(\omega)$ are the complex and frequency dependent compressional and shear velocities defined as

$$vc_p(\omega) = \sqrt{\frac{E(\omega)}{\rho}}, \quad vc_s(\omega) = \sqrt{\frac{\mu(\omega)}{\rho}} \tag{3}$$

with ρ the bulk density.

4.3 A viscoelastic model for wave propagation

The equation of motion in a 2D isotropic viscoelastic domain Ω with boundary $\partial\Omega$ is (Santos et al., 2011) :

$$\omega^2 \rho u + \nabla \cdot \sigma(u) = f(x, \omega), \quad \Omega, \tag{4}$$

with first-order absorbing boundary condition:

$$-\sigma(u)\nu = i\omega \mathcal{D} u, \quad \partial\Omega. \tag{5}$$

Here $f(x, \omega)$ is the external source and $\mathcal{D}$ is a positive definite matrix which definition is given in (Ha et al., 2002).

The numerical solution is computed at a selected number of frequencies in the range of interest using an iterative finite element domain decomposition procedure. The time domain solution is obtained using a discrete inverse Fourier transform (Ha et al., 2002) . To approximate each component of the solid displacement vector we employ a nonconforming finite element space which generates less numerical dispersion than the standard bilinear elements.

5 WAVE PROPAGATION EXAMPLES

5.1 2D Section Model

The simulated 2D section consists of a reservoir (such as the one described above) surrounded by an aquifer of high permeability (10 mD) and porosity (40%). For both we define fractal distributions of properties. The size of the whole section is 600 m $\times$ 400 m, at a depth of 2000 m. The bulk modulus of the dry matrix, K_m, is computed employing the Krief equation (Krief et al., 1990). Using the moduli K_s, K_m, μ_m, the porosity ϕ and permeability k, as well as the fluids bulk moduli and viscosities (computed using the Peng-Robinson model (Peng and Robinson, 1976)), we determine the complex and frequency dependent Lamé coefficients $\lambda(\omega), \mu(\omega)$ as explained before.

5.2 Experiments

Our fluid flow model allows us to get the position and time of occurrence of the different micro-seismic events. The seismic model takes this information and places a seismic source in each location, that produces a pulse at its corresponding time.

In this work, we test three different simplified experiments that only take into account three seismic sources. In each experiment, the sources are aligned in the same direction of each zone of weakness simulated above ($0°$, $45°$ and $90°$). We locate one source at the injection point (central source) and the other two equidistant, one on each side. The separation length between the central source and the others is the maximum distance reached by the micro-seismic event distribution. Since the micro-seismic events occur at different times, the central source emits first and the other two sources 200 ms later.

For the three scenarios we use an array of 160 receivers placed vertically along the right side of the simulated section.

First, we analyze the experiment where the sources are horizontally aligned. Figure 4 shows the horizontal traces detected by the receivers.

Three wave fronts arriving at different times are clearly observed. The shape of these fronts denotes the influence of the different rock properties between the reservoir and the aquifer. As Figure 5 shows, the P-wave phase velocity decreases as permeability and porosity increase.

The first wave front in Figure 4 corresponds to the central source that emits first. The other two wave fronts correspond to the other two sources that emit at the same time (200 ms later than the central source). Nevertheless, the delay of the signal arrival from these two sources is due to their different location respect to the receivers. The same behavior can be seen in Figures 6 and 7, where the snapshots of horizontal displacement at different times (50 ms and 250 ms) are shown.

Figure 6, corresponding to 50 ms, displays the front produced by the central source. In Figure 7, corresponding to 250 ms, only the wave fronts of the secondary sources can be appreciated, since the central source wave front reached the domain boundaries. The distance between the

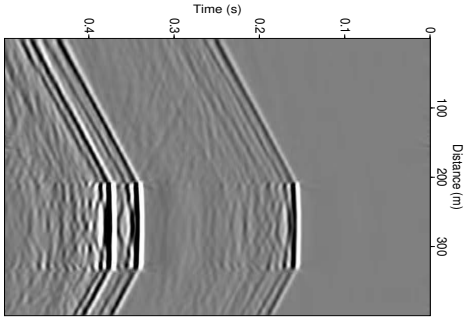

Figure 4: Horizontal velocity traces for sources aligned at 0°

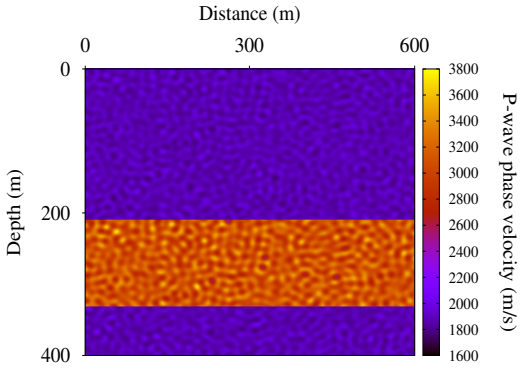

Figure 5: P-wave phase velocity map

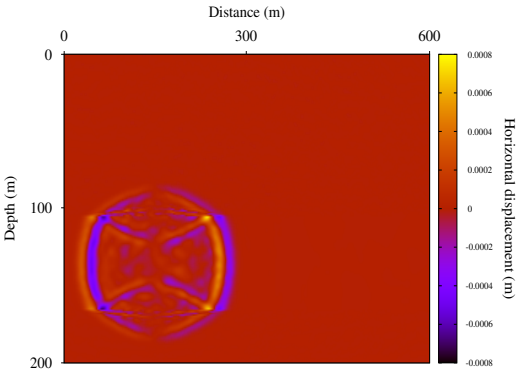

Figure 6: Snapshots of horizontal displacement at 50ms for sources aligned at 0°

two wave fronts observed in this figure causes the delay shown in Figure 4. Also, in these figures the reflections due to material property changes can be observed.

On the other hand, Figure 8 shows the horizontal traces obtained for the case with the sources aligned vertically. In this case only two wave fronts can be observed. The first due to the central source and the second one due to the other two sources. This conclusion can be driven from Figure 9 that shows the snapshot at 250 ms where both of these waves can be seen intersecting each other and generating a single wave front across the reservoir.

Finally, Figure 10 shows the horizontal traces obtained when the sources are aligned at a 45°

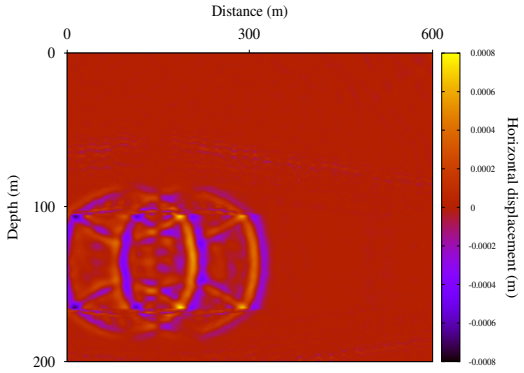

Figure 7: Snapshots of horizontal displacement at 250ms for sources aligned at 0°

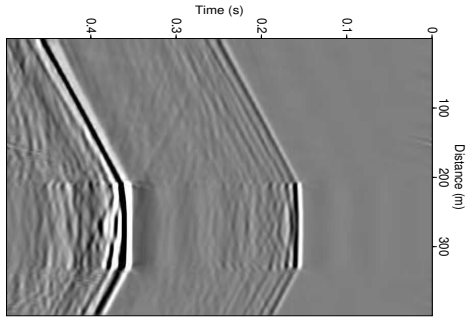

Figure 8: Horizontal velocity traces for sources aligned at 90°

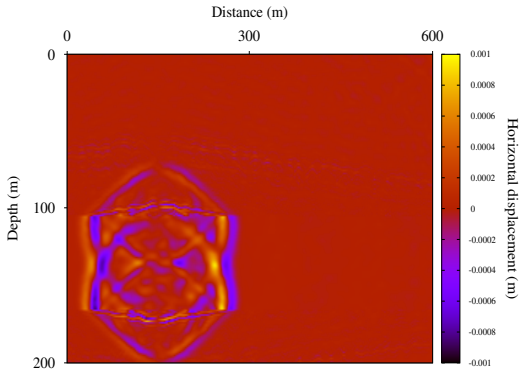

Figure 9: Snapshots of horizontal displacement at 250 ms for sources aligned at 90°

angle. Here we observe that the wave fronts generated by the two outmost sources are separated as in the first case, but are not parallel to each other. The same behavior can be seen in Figure 11 that displays the snapshot at 250 ms for this scenario.

6 CONCLUSIONS

In this study, our wave propagation model is used to reproduce seismograms generated from the capture of micro-seismic events produced during water injection in unconventional reservoirs.

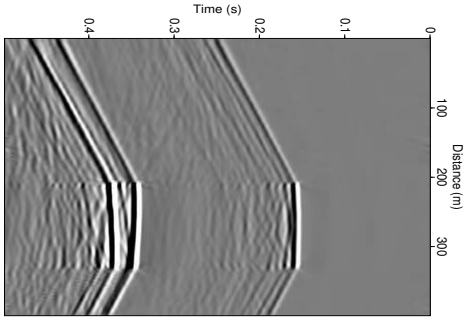

Figure 10: Horizontal velocity traces for sources aligned at $45°$

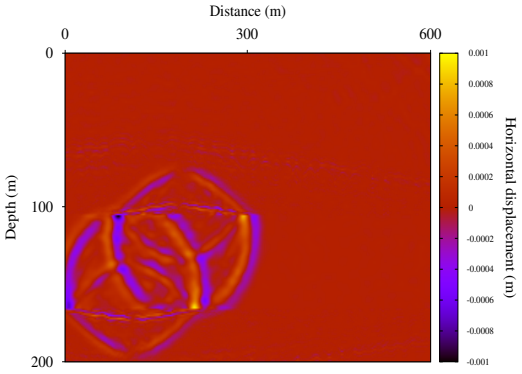

Figure 11: Snapshots of horizontal displacement at 250 ms for sources aligned at $45°$

The numerical experiments show the effect of different weak stress zones orientation over the synthetics seismograms.

These first results show the potential of the technique to detect the fracture orientation during water injection.

Furthermore, the combination of the wave propagation simulator with the fluid flow simulator allows to assess different fracturing strategies and maximize the information that can be obtained from seismograms.

REFERENCES

Aziz K. and Settari A. *Petroleum Reservoir Simulation*. Elsevier Applied Science Publishers, Great Britain, 1985.

Carcione J.M. and Gei D. Theory and numerical simulation of fluid-pressure diffusion in anisotropic porous media. *Geophysics*, 74:N31–N39, 2009.

Fanchi J. *Principles of Applied Reservoir Simulation*. Gulf Professional Publishing Company, Houston, Texas, 1997.

Ha T., Santos J., and Sheen D. Nonconforming finite element methods for the simulation of waves in viscoelastic solids. *Comput. Meth. Appl. Mech. Engrg.*, 191:5647–5670, 2002.

Krief M., Garat J., Stellingwerff J., and Ventre J. A petrophysical interpretation using the velocities of P and S waves (full waveform sonic). *The Log Analyst*, 31:355–369, 1990.

Nagel N., Zhang F., Sanchez-Nagel M., and Lee B. Quantitative evaluation of completion techniques on influencing shale fracture. *in Bunger, A., McLennan, J. and Jeffrey, R., eds, Effec-*

tive and Sustainable Hydraulic Fracturing, Brisbane, Australia, ISBN 978-953-51-1137-5, InTech, DOI: 10.5772/56304, pages 513–546, 2013.

Peng D.Y. and Robinson K. A new two-constant equation of state. *Ind. Eng. Chem. Fundam.*, 15:59–64, 1976.

Riahi A. and Damjanac B. Numerical study of interaction between hydraulic fracture and discrete fracture network. *in Bunger, A., McLennan, J. and Jeffrey, R., eds, Effective and Sustainable Hydraulic Fracturing, Brisbane, Australia, ISBN 978-953-51-1137-5, InTech, DOI: 10.5772/56304*, pages 271–286, 2013.

Rothert E. and Shapiro S.A. Microseismic monitoring of borehole fluid injections: Data modeling and inversion for hydraulic properties of rocks. *Geophysics*, 68:685–689, 2003.

Santos J.E., Carcione J.M., and Picotti S. Analysis of mesoscopic loss effects in anisotropic poroelastic media using harmonic finite element simulations. *Proc. 81th Annual International Meeting SEG (San Antonio)*, pages 2211–2215, 2011.

Savioli G. and Bidner M.S. Simulation of the oil and gas flow toward a well - a stability analysis. *Journal of Petroleum Science and Engineering*, 48:53–69, 2005.

Shapiro S.A., Huenges E., and Borm G. Estimating the crust permeability from fluid-injection-induced seismic emission at the KTB site. *Geophysics Journal International*, 131:F15–Fl8, 1997.

Shapiro S.A., Rentsch S., and Rothert E. Characterization of hydraulic properties of rocks using probability of fluid-induced micro-earthquakes. *Geophysics*, 70:F27–F33, 2005.

White J.E., Mikhaylova N.G., and Lyakhovitskiy F.M. Low-frequency seismic waves in fluid-saturated layered rocks. *Izvestija Academy of Siences USSR, Physics of Solid Earth*, 10:654–659, 1975.